Supplement of "Chemical ionization mass spectrometry utilizing benzene cations for measurements of volatile organic compounds and nitrogen oxide"

Uma Puttu[1], Jamie R. Kamp[1], Xiaoyu Chen[1], Jhao-Hong Chen[1], Jing Li[1], Miquel A Gonzalez-Meler[2], Jian Wang[1], and Lu Xu[1]

[1]Department of Energy, Environmental, and Chemical Engineering, Washington University in St. Louis, St. Louis, MO, USA
[2]Department of Biological Sciences, University of Illinois at Chicago, Chicago, IL, USA

Correspondence: Lu Xu (xu1@wustl.edu)

1 Instrument description

1.1 Benzene concentration entering IMR

The mixing ratio of benzene through the ion source is a critical parameter influencing reagent ion distribution and, consequently, analyte sensitivity. Previous studies have demonstrated this dependence; for example, Lavi et al. (2018) reported a significant decrease in isoprene sensitivity at benzene mixing ratios below 200 ppmv. Given its importance, and to enable comparison with other studies, we estimate the benzene mixing ratio through the ion source (i.e., entering the IMR) using two methods.

In the first method, we use the permeation rate of the benzene source. Two permeation tubes containing liquid benzene were employed to generate benzene vapor. Each tube was 20 cm long with a 0.3 cm inner diameter and emptied after approximately four months. This results in an estimated permeation rate of 7.3 μg min^{-1} per tube, or 14.6 μg min^{-1} combined. The benzene vapor was carried into the VUV source by a 400 sccm UHP N_2 flow. This yields a net benzene mixing ratio of approximately 10 ppmv in the reagent gas entering the IMR.

In the second method, we estimate the benzene concentration inside the IMR from reaction thermodynamics. This approach uses the equilibrium constant (K) between neutral benzene, $C_6H_6^+$, and $(C_6H_6)_2^+$ (Equation S1). The K is 13 Pa^{-1} at 308 K (Meot-Ner et al., 1978), which is the IMR temperature. Assuming equilibrium in the IMR, we can calculate the partial pressure of benzene ($P_{C_6H_6}$) from the measured reagent ion ratio, $C_6H_6^+/(C_6H_6)_2^+$. In this study, the observed mass spectrum peak ratio of $C_6H_6^+/(C_6H_6)_2^+$ is 5, assumed to be the same as in the IMR. This corresponds to a $P_{C_6H_6}$ of 1.5×10^{-2} Pa. At the IMR operating pressure of 55 mbar (5500 Pa), this partial pressure translates to a benzene concentration of 2.8 ppmv. Accounting for dilution of the reagent gas flow (400 sccm) by the sample flow (1800 sccm), the effective benzene mixing ratio through the ion source is approximately 15 ppmv, similar to the estimation from the first method. The benzene mixing ratio in our study is much lower than previous studies, which used on the order of 100 ppmv benzene through the ion source (Lavi et al., 2018; Schobesberger et al., 2023).

$$K = \frac{[(C_6H_6)_2^+]}{[C_6H_6^+]P_{C_6H_6}} \tag{S1}$$

1.2 Analyte classification

Table S1. Molecular mass, CAS#, Ionization energy (I.E), Proton affinity (PA), and $C_6H_6^+$ Affinity of analytes examined in this study and previous studies. This table lists analytes in "low IE class".

Compound	Composition	Mass	CAS#	I.E[a]	PA[a]	$C_6H_6^+$ Affinity
		amu		eV	kJ mol^{-1}	kJ mol^{-1}
N-Methylaniline	C_7H_9N	107.15	100-61-8	7.32	916.6	-
N-Ethylaniline	$C_8H_{11}N$	121.18	103-69-5	7.56	924.8	-
Aniline	$C_6H_5NH_2$	93.13	62-53-3	7.72	882.5	-
Diethylamine	$C_4H_{11}N$	73.14	109-89-7	7.90	952.4	-
4-Bromoanisole	C_7H_7BrO	187.03	104-92-7	8.13	-	-
Nalorphine	$C_{19}H_{21}NO_3$	311.37	62-67-9	8.15	-	-
4-Fluoroaniline	C_6H_6FN	111.12	371-40-4	8.18	871.5	-
Anisole	C_7H_8O	108.14	100-66-3	8.20	839.6	-
2-Methoxytoluene	$C_8H_{10}O$	122.16	578-58-5	8.24	850	-
β-Caryophyllene	$C_{15}H_{24}$	204.35	87-44-5	8.30	-	-
α-Humulene	$C_{15}H_{24}$	204.35	6753-98-6	8.35	-	-
α-Pinene	$C_{10}H_{16}$	136.23	80-56-8	8.35	863.2	143.4[b]
Ocimene	$C_{10}H_{16}$	136.12	13877-91-3	8.38	881.6	-
2-Methylfuran	C_5H_6O	82.04	534-22-5	8.38	865.9	-
1,3,5-TMB	C_9H_{12}	120.09	108-67-8	8.40	836.2	-
Tryptophan	$C_{11}H_{12}N_2O_2$	204.23	54-12-6	8.43	-	-
p-Xylene	C_8H_{10}	106.17	106-42-3	8.44	794.4	-
o-Cresol	C_7H_8O	108.14	95-48-7	8.46	800	-
Phenol	C_6H_6O	94.11	108-95-2	8.49	817.3	-
β-Myrcene	$C_{10}H_{16}$	136.12	123-35-3	8.50	854.4	-
tert-Butylamine	$C_4H_{11}N$	73.14	75-64-9	8.50	934.1	-
2-Chloroaniline	C_6H_6ClN	127.57	95-51-2	8.50	-	-
sec-Butylamine	$C_4H_{11}N$	73.14	13952-84-6	8.50	929.7	-
Isobutylamine	$C_4H_{11}N$	73.14	78-81-9	8.50	924.8	-
Limonene	$C_{10}H_{16}$	136.12	138-86-3	8.54	842	-
m-Xylene	C_8H_{10}	106.08	108-38-3	8.55	812.1	-
o-Xylene	C_8H_{10}	106.08	95-47-6	8.56	796	-
trans-1,3-Pentadiene	C_5H_8	68.12	2004-70-8	8.59	834.1	-
2-Chloroethyl ethyl sulfide	C_4H_9ClS	124.63	693-07-1	8.59	823	-
Isopropylamine	C_3H_9N	59.11	75-31-0	8.60	923.8	-
β-Pinene	$C_{10}H_{16}$	136.12	127-91-3	8.65	874	-

[a]I.E and PA values are from Linstrom et al. (1997). [b] $C_6H_6^+$ affinity for α-Pinene is from Vermeuel (2021).

Table S1. Continued for analytes in "mid IE class"

Compound	Composition	Mass amu	CAS#	I.E[a] eV	PA[a] kJ mol^{-1}	$C_6H_6^+$ Affinity kJ mol^{-1}
Benzene dimer	$C_{12}H_{12}$	156.00	-	8.69	-	-
Dimethyl sulfide	C_2H_6S	62.02	75-18-3	8.69	830.9	113.1[c]
4-Chlorotoluene	C_7H_7Cl	126.58	106-43-4	8.69	762.9	-
Butylbenzene	$C_{10}H_{14}$	134.22	104-51-8	8.69	791.9	-
Iodobenzene	C_6H_5I	204.01	591-50-4	8.72	-	-
n-Butylamine	$C_4H_{11}N$	73.14	109-73-9	8.73	921.5	-
Ethyl Benzene	C_8H_{10}	106.17	100-41-4	8.77	788	-
2-Methoxypyridine	C_6H_7NO	109.13	1628-89-3	8.82	934.7	-
Toluene	C_7H_8	92.06	108-88-3	8.83	784	-
2,6-Dimethylpyridine	C_7H_9N	107.15	108-48-5	8.86	963	-
Isoprene	C_5H_8	68.06	78-79-5	8.86	826.4	132.7[c]
Cyclohexene	C_6H_{10}	82.14	110-83-8	8.95	784.5	-
Bomobenzene	C_6H_5Br	157.01	108-86-1	9.00	754.1	-
Chlorobenzene	C_6H_5Cl	112.01	108-90-7	9.07	753.1	-
1,3 -Butadiene	C_4H_6	54.09	106-99-0	9.07	783.4	-
2-Methylpyridine	C_6H_7N	93.13	109-06-8	9.18	949.1	-
Flouorobenzene	C_6H_5F	96.10	462-06-6	9.20	755.9	-
D5 siloxane	$C_{10}H_{30}O_5Si_5$	370.77	541-02-6	-	-	

[a]I.E and PA values are from Linstrom et al. (1997). [c]$C_6H_6^+$ affinity for Dimethylsulfide and Isoprene are from Vermeuel (2021).

Table S1. Continued for analytes in "high IE class"

Compound	Composition	Mass	CAS#	I.E[a]	PA[a]	$C_6H_6^+$ Affinity
		amu		eV	kJ mol^{-1}	kJ mol^{-1}
Benzene	C_6H_6	78.11	71-43-2	9.24	750.4	74[d]
NO	NO	30.01	10102-43-9	9.26	531.8	184±21[e]
2-Iodopropane	C_3H_7I	169.99	75-30-9	9.40	-	-
2-Iodobutane	C_4H_9I	184.02	513-48-4	9.40	-	-
Benzaldehyde	C_7H_6O	106.12	100-52-7	9.50	834	-
MEK	C_4H_8O	72.11	78-93-3	9.52	827.3	-
1,4-Pentadiene	C_5H_8	68.12	591-93-5	9.62	-	-
MVK	C_4H_6O	70.04	78-94-4	9.65	834.7	-
2-Bromopyridine	C_5H_4BrN	158.00	109-04-6	9.70	904.8	-
Acetone	C_3H_6O	58.04	67-64-1	9.70	812	-
3-Chloropyridine	C_5H_4ClN	13.54	626-60-8	9.75	903.4	-
3-Bromopyridine	C_5H_4BrN	158.00	626-55-1	9.80	910	-
2-Chloropyridine	C_5H_4ClN	113.55	109-09-1	9.90	900.9	-
232 MBO	$C_5H_{10}O$	86.13	115-18-4	9.90	-	73.8[f]
MACR	C_4H_6O	70.04	78-85-3	9.92	808.7	-
Ammonia	NH_3	17.03	7664-41-7	10.07	853.6	78.7[g]
2-Propanol	C_3H_8O	60.09	67-63-0	10.17	793	-
Acrolein	C_3H_4O	56.03	107-02-8	10.11	797	-
4-Chloropyridine	C_5H_4ClN	113.55	626-61-9	10.20	916.1	-
Acetaldehyde	C_2H_4O	44.05	75-07-0	10.23	768.5	-
Ethanol	C_2H_6O	46.07	64-17-5	10.48	776.4	-
Methanol	CH_3OH	32.04	67-56-1	10.84	754.3	-
Acetonitrile	C_2H_3N	41.03	75-05-8	12.20	779.2	-
Hydrogen cyanide	HCN	27.03	74-90-8	13.60	712.9	-

[a]I.E and PA values are from Linstrom et al. (1997). $C_6H_6^+$ affinity for [d]Benzene is from Rusyniak et al. (2003), [e]NO from Reents and Freiser (1980), [f]232 MBO from Vermeuel (2021), and [g]Ammonia from Mizuse et al. (2010)

Table S2. Appearance energies of the selected analytes from NIST Chemistry WebBook.

Compound	Ion	Appearance Energy (eV)	Reference
Diethylamine (DEA)	$C_3H_8N^+$	8.92	Lossing et al. (1981)
	$C_3H_8N^+$	9.55	Collin and Franskin (1966)
Isopropylamine (IPA)	$C_2H_6N^+$	9.12	Lossing et al. (1981)
	$C_2H_6N^+$	8.86	Solka and Russell (1974)
	$C_3H_8N^+$	9.20	Lossing et al. (1981)
Limonene	$C_9H_{13}^+$	8.9	Harris et al. (1979)

1.3 Ion Chemistry from literature studies

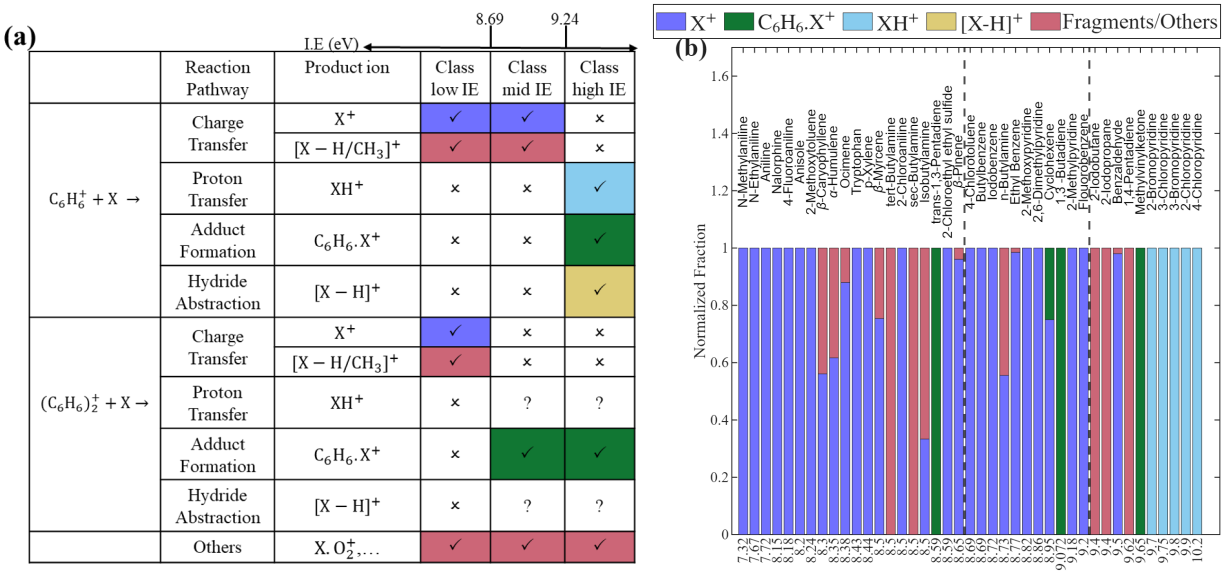

Figure S1. (a) Reaction pathways between reagent ions ($C_6H_6^+$ and $(C_6H_6)_2^+$) and analyte (X) across different analyte categories, along with the corresponding product ions observed in past studies. Symbols "✓", "✗", and "?" indicate high, low, and uncertain likelihood of the reaction, respectively. **(b)** Product ion distributions for each analyte, sorted by ionization energy (IE). The two vertical dashed lines mark the IE of 8.69 eV (benzene dimer) and 9.24 eV (benzene monomer). The same product ion formed via different reagent ions or ionization pathways are shown in the same color. Fragment ions from dissociative charge transfer and other reaction pathways are also shown in the same color, as they are difficult to distinguish experimentally.

In this study, we characterized the ionization pathways and product ion distributions for 27 analytes. Based on the results, we introduce a thermodynamics-based framework for the qualitative prediction of analyte's ion chemistry (Section 2.2). Our framework classifies analytes primarily by their IE, as this is the most widely available thermodynamic property in the liter-

ature. As additional thermodynamic data become available, these can be incorporated into the classification, enabling a more comprehensive and accurate prediction of ion chemistry and product ion distributions.

To further evaluate this framework's accuracy, we now apply it to a total of 41 analytes investigated in previous studies that used benzene cations as reagent ions (Subba Rao and Fenselau, 1978; Allgood et al., 1990; Ketkar et al., 1991; Leibrock et al., 2003; Kim et al., 2016; Lavi et al., 2018; Miller and Gross, 1983). We note that direct quantitative comparison between these different studies is challenging, due to variations in instrumental conditions, including voltage gradients, IMR operating conditions, and reagent ion distributions.

20 of the 41 analytes fall into "low IE class". For 19 of these 20 analytes, charge transfer is the sole ionization pathway, consistent with our proposed framework. For these 19 analytes, 11 analytes have the molecular ion (X^+) as the predominant product ion, 3 analytes (tert-Butylamine, sec-Butylamine, and Iso-Butylamine) undergo dissociative charge transfer as their low appearance energies (AE) is smaller than 9.24 eV (Allgood et al., 1990), and 5 analytes (β-Caryophyllene, α-Humulene, Ocimene, β-pinene, and β-Myrcene) form additional product ions due to secondary ion chemistry involving O_2. In this class, the sole outlier contrary to our framework is trans-1,3-pentadiene from Leibrock and Huey (2000), which reported the formation of adduct ion ($C_{11}H_{14}^+$). The reason for the discrepancy is unknown, but may be due to from different instrument conditions. For example, in Leibrock and Huey (2000), the only reagent ion is $(C_6H_6)_2^+$, whereas both $(C_6H_6)^+$ and $(C_6H_6)_2^+$ exist in our study. The IE of trans-1,3-pentadiene is 8.59 eV, which is only slightly lower than that of benzene dimer (i.e., 8.69 eV).

11 of the 41 analytes fall into "mid IE class". For 8 of these, the molecular ion formed via charge transfer reaction is the sole product, consistent with our proposed framework. A fragment ion is observed for n-butylamine, as its AE is lower than 9.24 eV (Allgood et al., 1990). Two analytes, cyclohexene and 1,3-butadiene, appear to be contrary to our framework. For cyclohexene, Leibrock and Huey (2000) observed both molecular ion and adduct ion, even though $(C_6H_6)_2^+$ was the only reagent ion in that study. Under this condition, our framework predicts adduct ion as the sole product. We hypothesize that the molecular ion is from declustering of the adduct ion in the ion optics, rather than being formed in the IMR. For 1,3-butadiene, Holman et al. (1986) only observed adduct ion, even though $C_6H_6^+$ was claimed to be the only reagent ion in that study. Under this condition, our framework predicts charge transfer ion as the sole product. We hypothesize that the actual reagent ion in Holman et al. (1986) was $(C_6H_6)_2^+$, which fragments in the CID cell and produced the $C_6H_6^+$. 10 of the 41 analytes fall into the "high IE class". 9 of the 10 analytes react primarily via proton transfer, adduct formation, or other reactions. Proton transfer was the dominant pathway for five substituted pyridines, which all have higher PA than phenyl radical. Adduct formation was observed for methyl vinyl ketone upon its reaction with $(C_6H_6)_2^+$. For 2-iodopropane and 2-iodobutane, Miller and Gross (1983) suggested a unique reaction, where $C_6H_6^+$ reacts with both analytes, displaces an iodine atom, and produces $C_9H_{13}^+$ and $C_{10}H_{15}^+$, respectively. Analyte 1,4-pentadiene produced an ion at *m/z* 68 when reacted with $C_6H_6^+$, where its chemical formula could not be assigned. The only exception to our framework is benzaldehyde, which showed a molecular ion in the study by Leibrock and Huey (2000). However, in a different study, Stone and Lin (1980) only observed adduct ion for benzaldehyde. Therefore, we hypothesize that the molecular ion observed by Leibrock and Huey (2000) was likely formed from the declustering of the initially formed adduct ion.

We note that, among all analytes examined in this study and in the literature, protonated ions were observed only for five substituted pyridines. The infrequent occurrence of protonated ions is likely because of the high threshold for proton transfer, defined by the phenyl radical proton affinity (PA, 884 kJ mol^{-1}). After reviewing the proton affinities of more than 470 analytes compiled by Pagonis et al. (2019), we find that only 29 amines exceeded the PA of the phenyl radical. These results suggest that proton transfer is generally unlikely for atmospheric VOCs. However, we note that the compiled analytes are primarily VOCs and small OVOCs, so the potential for proton transfer among larger or more complex OVOCs remains uncertain.

1.4 Mass-Dependent Transmission Efficiency

As shown in previous studies (Krechmer et al., 2018; Xu et al., 2022), the BSQ functions as a high-pass filter, with reduced transmission efficiency (TE) at lower *m/z*. We estimated the mass-dependent TE using an experiment in which polyethyleneimine (PEI) was heated to 100°C under N_2. The PEI emitted numerous species spanning *m/z* 40–160, causing the observed total ion counts (TIC), calculated using Equation S2, to vary by nearly 20% (Figure S2a). We estimate the mass-dependent TE from the observed signals at each *m/z* ($I_{m/z}$), based on the principle that the TIC after correcting for mass-dependent TE ($\mathrm{TIC_{corrected}}$) should remain constant (Equation S3). We model the *m/z* - TE relationship with a logistic function (Equation S4). The parameter a is fixed as 1 to represent the maximum TE. We then perform optimization by minimizing the variability of the $\mathrm{TIC_{corrected}}$ time series, where the variability is defined as (max–min)/mean. The optimized parameter values for b and c were 0.31 and 63, respectively (Figure S2b). The resulting $\mathrm{TIC_{corrected}}$ time series is shown in Figure S2a, and the mass-dependent TE curve is shown in Figure S2c.

$$\mathrm{TIC_{observed}} = \sum_{m/z=40}^{160} I_{m/z} \tag{S2}$$

$$\mathrm{TIC_{corrected}} = \sum_{m/z=40}^{160} \frac{I_{m/z}}{\mathrm{TE}_{m/z}} = \text{constant} \tag{S3}$$

$$\mathrm{TE} = \frac{\mathrm{a}}{1 + exp(-\mathrm{b}(m/z - \mathrm{c}))} \tag{S4}$$

2 Instrument Performance

2.1 Comparison of sensitivities between instruments

We compare the absolute sensitivities obtained in this study with those reported in previous benzene CIMS studies (Figure S3). Most prior studies report only normalized sensitivities (in ncps pptv^{-1}) and the comparison is shown in Figure S3b. We also attempt to compare the absolute sensitivity (in cps pptv^{-1}) by multiplying the normalized sensitivity and the total reagent ion counts, if available (Table S3).

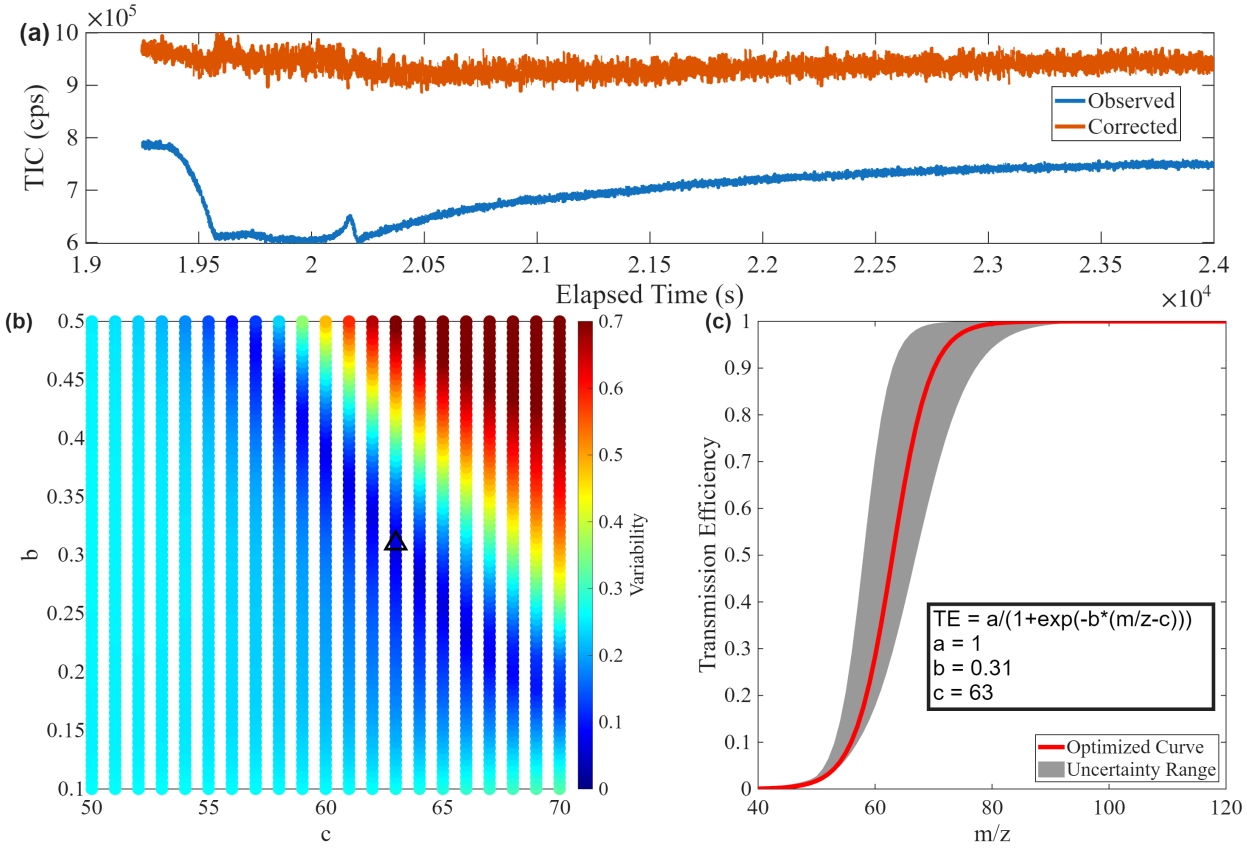

Figure S2. (a) Time series of observed TIC (Equation S2) and corrected TIC (Equation S3). (b) Parameters b and c, color-coded by variability in the $TIC_{corrected}$ time series. The △ represents the optimum point with minimum variability in the corrected TIC. The variability is defined as (max TIC – min TIC) / mean TIC. (c) Transmission efficiency as a function *m/z*. The red line represents the optimized transmission efficiency and the shaded area represents the uncertainty range.

For DMS, the compound most frequently quantified using benzene CIMS, our sensitivity is comparable to that reported by Schobesberger et al. (2023) but approximately three times lower than the value in Kim et al. (2016). This discrepancy is partly due to differences in product ion distributions. In our study, DMS forms both adduct and charge transfer ions with roughly equal intensity, whereas in Kim et al. (2016), only a single product ion was detected. Mungall et al. (2016) reported a DMS sensitivity of 80±30 cps $pptv^{-1}$, substantially higher than in other studies, with no clear explanation for such high sensitivity.

For isoprene, the sensitivity based on the $C_{11}H_{14}^+$ adduct ion is similar to those reported in Schobesberger et al. (2023) and Lavi et al. (2018), but lower by a factor of 7 than Kim et al. (2016).

Our measured sensitivity for NH_3 (1.64 cps $pptv^{-1}$) is similar to that reported in Schobesberger et al. (2023) (1.35 cps $pptv^{-1}$). For limonene, our measured sensitivity is seven times higher than that reported by Lavi et al. (2018). This difference is likely due to the dominant reagent ion: $C_6H_6^+$ in our study vs. $(C_6H_6)_2^+$ in the previous one. Since charge transfer reactions

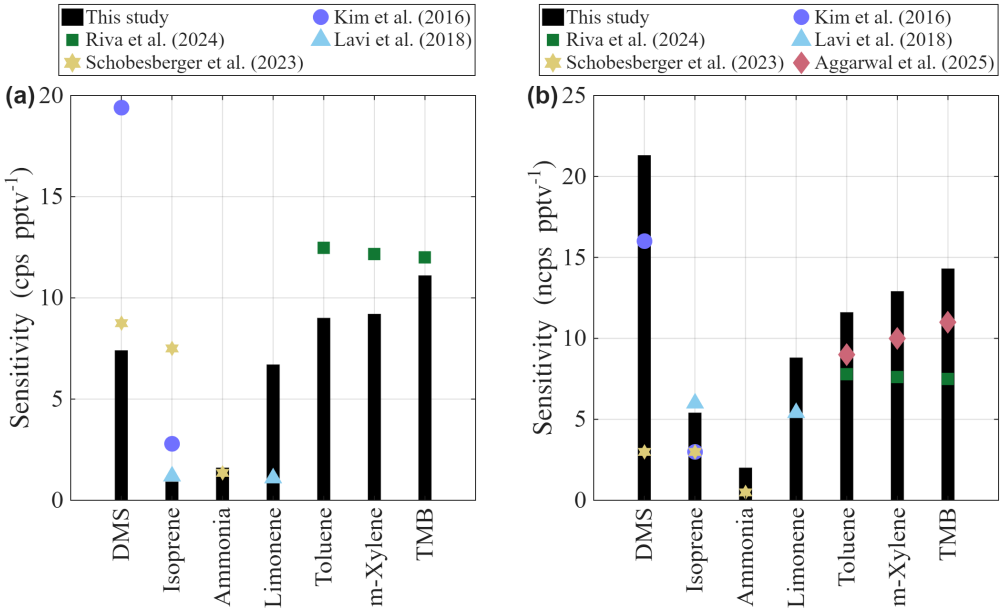

Figure S3. Comparison of (a) absolute sensitivities (b) normalized sensitivities, between this study and previous studies using benzene CIMS. Absolute sensitivities are directly reported in this study and in Kim et al. (2016), while values from other studies are estimated based on reported normalized sensitivities and total reagent ion counts. Note that Schobesberger et al. (2023) employed deuterated benzene as the reagent gas.

proceed more efficiently with $C_6H_6^+$ than with $(C_6H_6)_2^+$, as inferred from the α and β values of limonene (Table 1), the higher abundance of $C_6H_6^+$ in our system leads to enhanced sensitivity. Compared to Riva et al. (2024), which used the same IMR as our setup, our sensitivities for overlapping analytes, toluene, m-xylene, and trimethylbenzene, are slightly lower, likely due to lower reagent ion signal in this study (Table S3). Overall, these comparisons highlight the influence of reagent ion distribution on instrument sensitivity.

Table S3. IMR pressure, normalized sensitivity, normalization method, reagent ion counts, $C_6H_6^+/(C_6H_6)_2^+$ ratio and sensitivity for analytes from previous studies utilizing benzene cations.

Study	IMR pressure (mbar)	Analyte	Normalized sensitivity (ncps pptv^{-1})	Normalization method	Reagent ion counts (cps)	$C_6H_6^+/(C_6H_6)_2^+$	Absolute sensitivity (cps pptv^{-1})
This study	55	-	-	$C_6H_6^+ + \beta/\alpha\ (C_6H_6)_2^+$	7.8×10^5	5	-
Aggarwal et al. (2025) [a]	50	-	-	$C_6H_6^+ + (C_6H_6)_2^+$	-	-	-
Riva et al. (2024)	50	Toluene	7.8	$C_6H_6^+ + (C_6H_6)_2^+$	1.6×10^6	-	12.5
		m-Xylene	7.6	$C_6H_6^+ + (C_6H_6)_2^+$	1.6×10^6	-	12.2
		1,2,4 TMB	7.5	$C_6H_6^+ + (C_6H_6)_2^+$	1.6×10^6	-	12
Schobesberger et al. (2023) [b]	100	Ammonia	0.5	$C_6D_6^+$	2.5×10^6	6	7.5
		DMS	3.5	$C_6D_6^+$	2.5×10^6	6	8.75
		Isoprene	3	$C_6D_6^+$	2.5×10^6	6	1.25
Lavi et al. (2018)	75	Isoprene	6	$C_6H_6^+ + (C_6H_6)_2^+$	0.2×10^6	33	1.2
		Limonene	5.4	$C_6H_6^+ + (C_6H_6)_2^+$	0.2×10^6	33	1.1
Kim et al. (2016)	70	DMS	15	$C_6H_6^+ + (C_6H_6)_2^+$	2.5×10^6	3.3×10^{-4}	19.4
		Isoprene	3	$C_6H_6^+ + (C_6H_6)_2^+$	2.5×10^6	3.3×10^{-4}	2.8
Mungall et al. (2016)	100	DMS	-	-	-	-	80 ± 30

[a] Aggarwal et al. (2025) only reported the normalized sensitivities. [b] Schobesberger et al. (2023) reported a range of $2-3 \times 10^6$ cps for reagent ion count. We use the average value here. The normalization method is not specified, and we assume it to be $C_6D_6^+$, which was used to normalize the signal of NH_3 in that study.

2.2 LoD and Precision

In addition to sensitivity, an instrument's performance is also characterized by its precision and its Limit of Detection (LoD). The LoD is the lowest concentration of an analyte that an instrument can reliably detect, defined as extent to which the gross analyte signal (S_t) exceeds the background signal (S_b). The relation between S_t and S_b can be expressed as follows (MacDougall et al., 1980):

$$S_t - S_b \geq K_d \sigma \tag{S5}$$

Here, σ is the standard deviation of background count rates. We follow the typical convention of setting $K_d = 3$, which places the LoD at three standard deviations (3σ) above the background signal. To apply this, we first determine the instrument background counts by sampling UHP N_2. We then derive the LoD, expressed in mixing ratios (pptv), from the normalized sensitivities for various species. The calculated detection limits of 14 analytes characterized in the laboratory are listed in Table 1.

The precision of the benzene CIMS is defined as the standard deviation of the Gaussian fit to the normalized distribution of the normalized adjacent differences (NAD). We calculate the NAD for 15 minutes of measurement at 1 Hz, maintaining constant analyte mixing ratios, based on Equation S6 (Bertram et al., 2011).

$$\text{NAD} = \frac{[X]_n - [X]_{n-1}}{\sqrt{[X]_n [X]_{n-1}}} \tag{S6}$$

2.3 Absolute and normalized sensitivity

Table S4. Multi-component calibration mixture in nitrogen for the two VOC cylinders used in this study.

Standard Compound	Cylinder #	Formula	CAS (#)	Concentration (ppbv)	Uncertainty (%)
Acetonitrile	1	C_2H_3N	75-05-8	980	± 5
Acrolein	1	C_3H_4O	107-02-8	991	± 5
Methyl Ethyl Ketone	1	C_4H_8O	78-93-3	1027	± 5
Benzene	1	C_6H_6	71-43-2	1000	± 5
o-Xylene	1	C_8H_{10}	95-47-6	1003	± 5
Chlorobenzene	1	C_6H_5Cl	108-90-7	984	± 5
1,3,5-Trimethyl benzene	1	C_9H_{12}	108-67-8	1001	± 5
Phenol	1	C_6H_6O	108-95-2	493	± 5
Limonene	1	$C_{10}H_{16}$	138-86-3	974	± 5
Dimethylcyclopentasiloxane	1	$C_{10}H_{30}O_5Si_5$	541-02-6	1010	± 5
Hydrogen Cyanide	2	HCN	74-90-8	1017	± 5
Acetaldehyde	2	C_2H_4O	75-07-0	1092	± 5
m-Xylene	2	C_8H_{10}	108-38-3	995	± 5
o-Cresol	2	C_7H_8O	95-48-7	513	± 5
2-Methyl furan	2	C_5H_6O	543-22-5	985	± 5
Dimethyl sulfide	2	C_2H_6S	75-18-3	1029	± 5
Isoprene	1 & 2	C_5H_8	78-79-5	1017	± 5
Methacrolein	1 & 2	C_4H_6O	78-85-3	951	± 5
Toluene	1 & 2	C_7H_8	108-88-3	986	± 5
Acetone	1 & 2	C_3H_6O	67-64-1	1024	± 5

Table S5. Comparisons of slopes and R^2 for different normalization schemes using St. Louis data.

Normalization Scheme	Isoprene (CIMS vs GC)		NO (CIMS vs Gas Analyzer)	
	Slope	R^2	Slope	R^2
$C_6H_6^+$	0.85	0.98	0.97	0.92
$(C_6H_6)_2^+$	0.92	0.99	0.62	0.94
$C_6H_6^+ + (C_6H_6)_2^+$	0.86	0.98	0.85	0.93
$C_6H_6^+ + \beta/\alpha\ (C_6H_6)_2^+$	0.92	0.99	0.97	0.92
$\alpha/\beta\ C_6H_6^+ + (C_6H_6)_2^+$	0.93	0.99	-	-

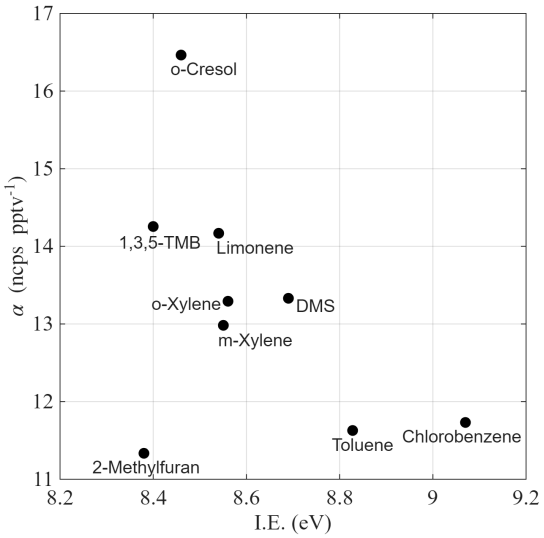

Figure S4. α (ncps pptv^{-1}) as a function of IE for the charge transfer product ions. D5-siloxane is excluded due to its unknown IE. Isoprene is excluded due to fragmentation.

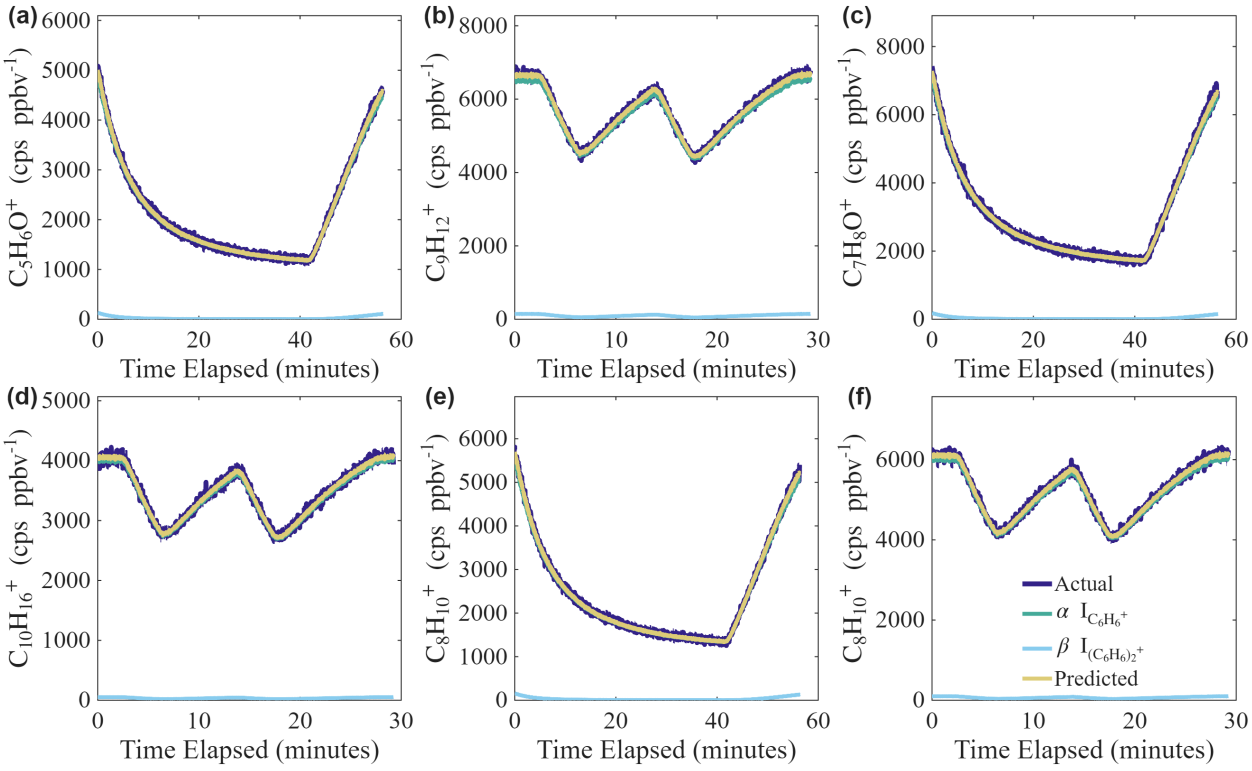

Figure S5. Estimation of α and β by varying the reagent ions $C_6H_6^+$ and $(C_6H_6)_2^+$ concentrations for analytes in low IE class. (a) 2-Methylfuran (b) 1,3,5 TMB (c) o-Cresol (d) Limonene (e) m-Xylene (f) o-Xylene.

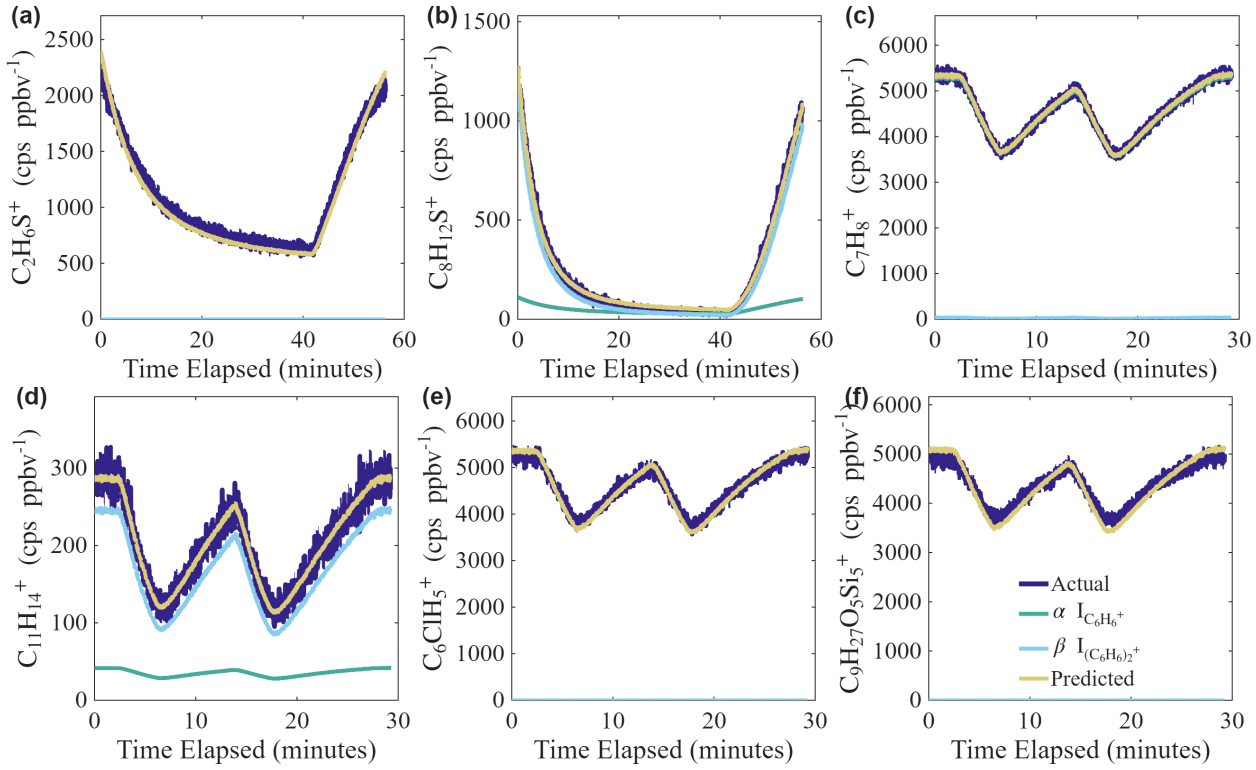

Figure S6. Estimation of α and β by varying the reagent ions $C_6H_6^+$ and $(C_6H_6)_2^+$ concentrations for analytes in mid IE class. (a) DMS (b) DMS adduct (c) Toluene (d) Isoprene adduct (e) Chlorobenzene (f) D5 siloxane. The α $I_{C_6H_6^+}$line is not shown for the analytes Chlorobenzene and D5 siloxane, because of $\beta = 0$ where the green line completely overlaps with yellow.

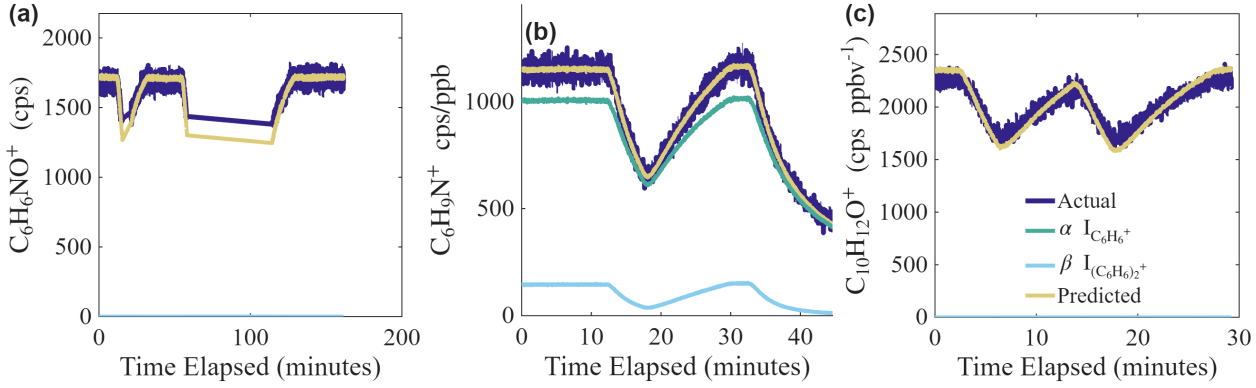

Figure S7. Estimation of α and β by varying the reagent ions $C_6H_6^+$ and $(C_6H_6)_2^+$ concentrations for analytes in high IE class. (a) NO (b) Ammonia (c) MACR. The α $I_{C_6H_6^+}$line is not shown for the analytes NO and MACR, because of $\beta = 0$ where the green line completely overlaps with yellow.

We introduce a method to calculate the normalized sensitivity (Equation 4), which accounts for the different contributions from $C_6H_6^+$ and $(C_6H_6)_2^+$. This consideration is important when the relative abundances of the two reagent ions vary over time, or when their distributions differ between calibration and deployment. To illustrate, we applied four different normalization methods to the St. Louis deployment and evaluated the accuracy of different normalization methods by comparing them to co-located measurements of isoprene and NO. As shown in Table S5, our method produced the best agreement. For isoprene, Equation 4 results in equally excellent results as normalizing to $(C_6H_6)_2^+$ alone. This is consistent with the fact that $(C_6H_6)_2^+$ is the major reagent ion forming the isoprene product ion $C_{11}H_{14}^+$. In contrast, normalizing by $C_6H_6^+$ alone or by the sum of $C_6H_6^+$ and $(C_6H_6)_2^+$ led to equally poor agreement. This is because $C_6H_6^+$ is not the dominant reagent ion, yet its signal is much higher than that of $(C_6H_6)_2^+$, thus overwhelming the summed normalization. Similar behavior was observed for NO. Therefore, it is preferable to identify the reagent ion responsible for each product ion and apply the corresponding normalization method. If this information is not available, normalizing by the sum of $C_6H_6^+$ and $(C_6H_6)_2^+$ is an acceptable fallback, but the potential limitations of this approach should be kept in mind.

2.4 Instrument operating conditions

We investigate the effects of IMR temperature, IMR pressure, and flow rate of reagent gas on analyte sensitivities. The experiments were conducted by varying one parameter at a time while keeping the others, along with voltages, constant. To investigate the impact of reagent gas flow rate on analyte sensitivity, we conducted experiments varying the flow from 50 sccm to 600 sccm. As shown in Figure S8a, the sensitivities of all analytes initially increase with reagent gas flow but begin to decrease when the flow exceeds about 350 sccm. This non-monotonic trend likely arises from competing effects between reagent gas abundance and ion–molecule reaction time. At low flow rates, increasing the flow rate enhances benzene abundance in the VUV source, leading to higher concentrations of reagent ions in the IMR and thus greater sensitivity. However, at higher flow rates, the benefit of increased reagent ion production becomes smaller, while the higher flow rate reduces ion–molecule reaction time, leading to decreased sensitivity.

We examine the dependence of sensitivity on IMR pressure by varying the pressure from 37 mbar to 70 mbar. As shown in Figure S8b sensitivities of all analytes increase with pressure. This trend is in consistent with findings of Riva et al. (2024) and Aggarwal et al. (2025), both of which used the same IMR as in this study. The increase in sensitivity at higher pressure is due to enhanced collision frequency. As the IMR pressure increases, the number density of both analyte molecules and reagent ions increases, leading to more ion-molecule collisions and thus higher sensitivity.

The effect of IMR temperature varies with analyte ionization pathways. As shown in Figure S9a, analytes ionized through charge transfer (i.e., low and mid IE classes), exhibit a 20% decrease in absolute sensitivity as the temperature increases from 30°C to 70°C. Figure S9b shows analytes ionized via adduct formation (i.e., mid and high IE classes). In this group, adduct ions of isoprene, NH_3, and DMS show substantial decreases in sensitivity with rising temperature, while those of NO and MACR show relatively small change.

IMR temperature can influence analyte sensitivity by affecting the ion–molecule collision rate, reaction time, and reagent ion distribution. Using the parameterization by Su (1994), we estimate that the collision rate constant changes by only 2% over

the 30°C to 70°C range, suggesting a minimal direct impact on sensitivity from this factor alone. Increasing IMR temperature reduces ion–molecule reaction time. At constant reagent and sample flow rates, a higher IMR temperature requires a greater pumping flow at the reactor exit to maintain constant IMR pressure, thereby shortening the residence time and decreasing sensitivity. Aggarwal et al. (2025) estimated a roughly 20% decrease in reaction time when IMR temperature increases from 30°C to 100°C, consistent with the observed sensitivity drop for charge transfer ions in Figure S9a.

Temperature also alters reagent ion distribution. As IMR temperature rises, the signal of $(C_6H_6)_2^+$ continuously decreases (Figure S9b), likely due to thermal fragmentation of this weakly bound adduct. In constrast, the temperature effect on $C_6H_6^+$ is weaker. Its signal initially increases with temperature and then plateaus near 60°C (Figure S9a). The initial increase in $C_6H_6^+$ may result from the thermal fragmentation of $(C_6H_6)_2^+$. The distinct temperature trends of $C_6H_6^+$ and $(C_6H_6)_2^+$ affect analyte sensitivities depending on their dominant ionization pathway. For example, the sensitivities of isoprene, NH_3, and DMS adduct ions, which primarily arise from reactions with $(C_6H_6)_2^+$, as indicated by their larger β than α values (Table 1), decrease with increasing temperature, mirroring the trend of $(C_6H_6)_2^+$. In contrast, the NO and MACR adduct ions, which are mainly formed via reactions with $C_6H_6^+$, exhibit much weaker temperature dependence, consistent with the trend of $C_6H_6^+$.

Based on the results above, we recommend an IMR pressure of 55 mbar, an IMR temperature of 35 °C, and a reagent gas flow rate of 350-400 sccm. Although higher IMR pressure generally yields higher sensitivity, a lower pressure is chosen to balance sensitivity with pump longevity. The reactor temperature is set slightly above ambient to ensure temperature control without losing too much sensitivity.

The two product ions of DMS exhibit different trends with changing IMR temperature. The signal of the charge transfer ion $C_2H_6S^+$ remains relatively stable, whereas the adduct ion $C_8H_{12}S^+$ decreases substantially as temperature increases. This is likely because $C_8H_{12}S^+$ is a weakly bound adduct, which undergoes thermal fragmentation at higher temperatures. The resulting fragments include $C_2H_6S^+$, which may help maintain its signal, contributing to its relatively weak temperature dependence.

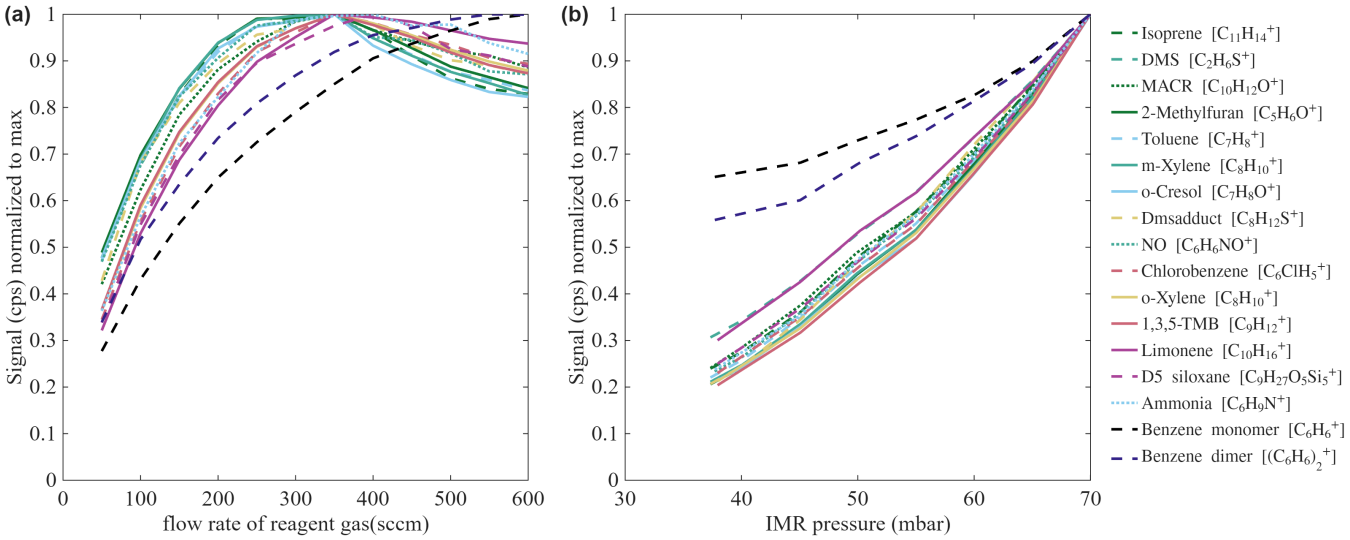

Figure S8. Effects of instrument operating conditions on analyte sensitivity: (a) reagent gas flow rate and (b) IMR pressure. Solid, dashed, and dotted lines represent analytes in low, mid, and high IE classes, respectively. Analyte signals are normalized to their maximum values within each test.

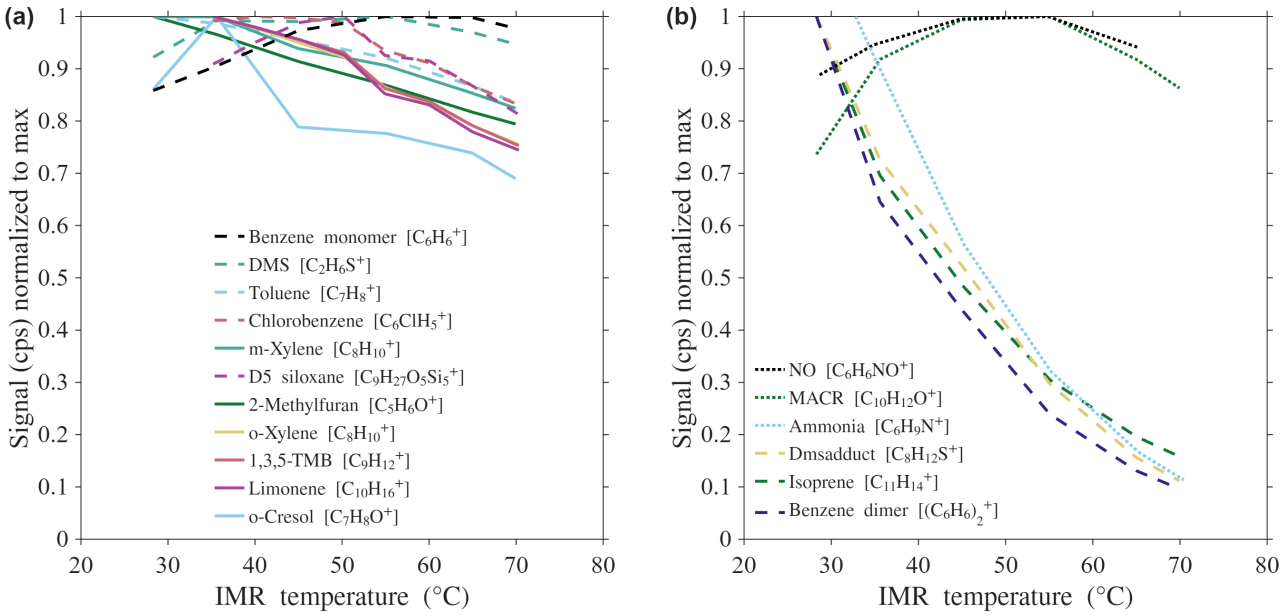

Figure S9. Effects of IMR temperature on analyte sensitivity: (a) charge transfer ions and (b) adduct ions. Solid, dashed, and dotted lines represent analytes in low, mid, and high IE classes, respectively. Analyte signals are normalized to their maximum values within each test.

2.5 Humidity dependence of reagent ions

Water level affects reagent ion distributions in benzene CIMS and subsequently influences analyte sensitivity (Section 3.3). As the water mixing ratio increases, the signal of $C_6H_6^+$ decreases by only 5%, whereas the signal of $(C_6H_6)_2^+$ shows a weak initial increase followed by a significant decrease (Figure S10a). These trends can be explained by ion chemistry between reagent ions and neutral water clusters. At low water mixing ratios (<0.3%), $C_6H_6^+$ reacts with water monomers to form $C_6H_6(H_2O)^+$, while larger neutral water clusters can be ignored due to their low abundance. The $C_6H_6(H_2O)^+$ can be replaced by benzene to form $(C_6H_6)_2^+$, as the affinity of $C_6H_6^+$ for H_2O is lower than that for benzene. As a result, the $C_6H_6^+$ signal decreases while the $(C_6H_6)_2^+$ signal increases. At higher humidity (>0.3%), the abundance of larger water clusters, such as trimers and tetramers, increases, and these clusters can compete with benzene in reactions with $C_6H_6^+$. Consequently, a larger fraction of $C_6H_6^+$ reacts with water clusters to form $C_6H_6(H_2O)_3^+$ and $C_6H_6(H_2O)_4^+$ instead of forming $(C_6H_6)_2^+$, leading to a decrease in the $(C_6H_6)_2^+$ signal. The relatively stable $C_6H_6^+$ signal is less well understood, but may be due to partial declustering of $C_6H_6(H_2O)_3^+$ and $C_6H_6(H_2O)_4^+$ back to $C_6H_6^+$. If this declustering occurs downstream of the IMR, the observed $C_6H_6^+$ signal may not reflect its true abundance in the IMR. In other words, although the observed $C_6H_6^+$ signal appears relatively stable, the actual $C_6H_6^+$ abundance in the IMR may still decrease with increasing water mixing ratio.

Table S6. Ionization energy (IE), $C_6H_6^+$ affinity, proton affinities and reaction enthalpy of dissociative proton transfer (DPT) reaction for the water clusters $(H_2O)_n$ for n = 1 to n = 6

$(H_2O)_n$	I.E[a]	$C_6H_6^+$ affinity[b]	Proton Affinity[b]	Reaction enthalpy of DPT reaction[b]
	eV	kJ mol^{-1}	kJ mol^{-1}	kJ mol^{-1}
1	12.81	37.66	691	96.23
2	11.88	58.58	813	41.84
3	11.93	72.13	880	0
4	11.55	79.49	930	-12.55
5	11.31	87.86	955	-20.92
6	11.40	86.86	968	-

[a]IE values are from Tomoda and Kimura (1983). [b]$C_6H_6^+$ affinity, Proton Affinity and Reaction enthalpy of DPT reaction values are from Ibrahim et al. (2005).

2.6 Voltage scanning

To investigate the relative binding energies and stability of different product ions, we employed the voltage scanning method (Lopez-Hilfiker et al., 2016; Xu et al., 2022; Aggarwal et al., 2025). Following the procedure of Aggarwal et al. (2025), the voltage gradient (ΔV) between the skimmer and BSQ front was varied in 1 V increments, while the voltage between the BSQ front and back was held constant. Increasing ΔV raises collisional energy, enhancing collision-induced dissociation (CID) and thereby reducing the signal intensity of weakly bound adduct ions. As shown in Figure S14a, the signals of all charge-transfer

Table S7. Binding energies of water clusters ions for n = 2 to n = 6

Cluster ion $H^+(H_2O)_n$	Binding Energy[a] kJ mol^{-1}
2	136 ± 9
3	84 ± 5
4	73 ± 4
5	56 ± 20
6	50 ± 8

[a] Binding energy values are from Lin-strom et al. (1997).

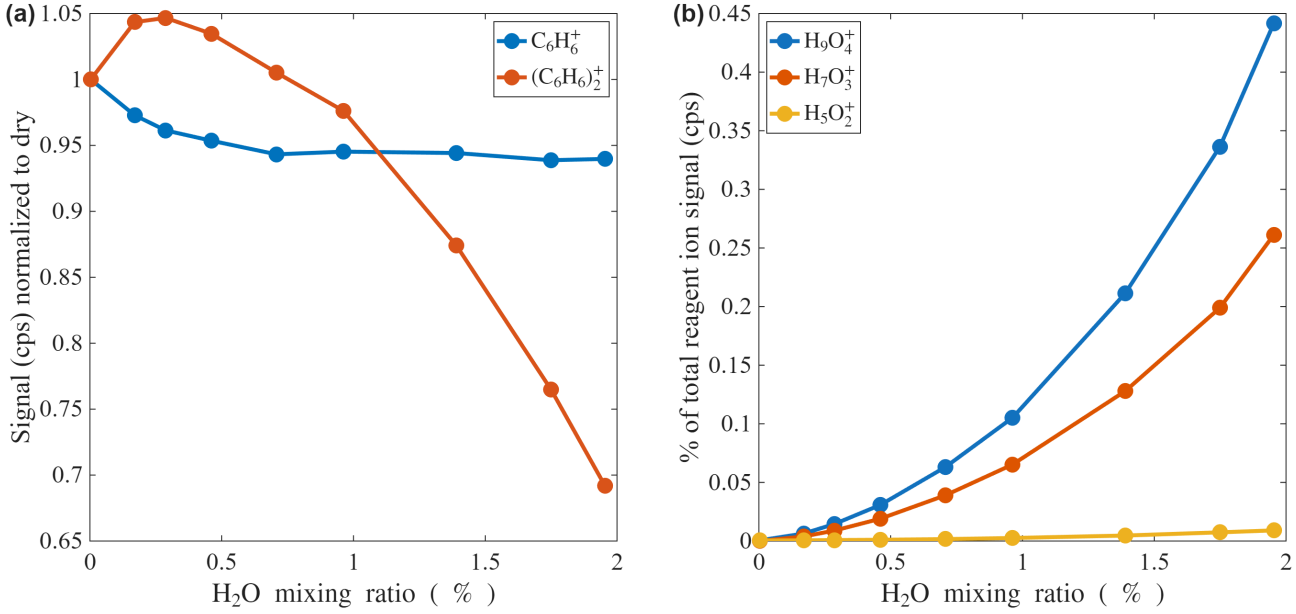

Figure S10. Dependence of (a) reagent ion signals and (b) water cluster ion signals on water mixing ratio.

ions, except for D5-siloxane, remain constant with increasing ΔV, consistent with the expected stability of molecular ions. In contrast, most adduct ions, including $(C_6H_6)_2^+$, $C_8H_{12}S^+$, $C_6H_9N^+$, $H_9O_4^+$, and $H_7O_3^+$, exhibit large signal decreases (Figure S14b). Interestingly, three adduct ions ($C_6H_6NO^+$, $C_{11}H_{14}^+$, and $C_{10}H_{12}O^+$) show only moderate decreases. This may be due to that these adduct ion are not weakly bound ion-dipole clusters but instead covalently bonded ion adducts. This hypothesis is supported by prior studies: Sieck and Gorden (1976) reported that $C_6H_6NO^+$ adopts a covalently bonded structure similar to nitrosobenzene, and Holman et al. (1986) demonstrated that 1,3-butadiene undergoes cycloaddition with $C_6H_6^+$ to form a

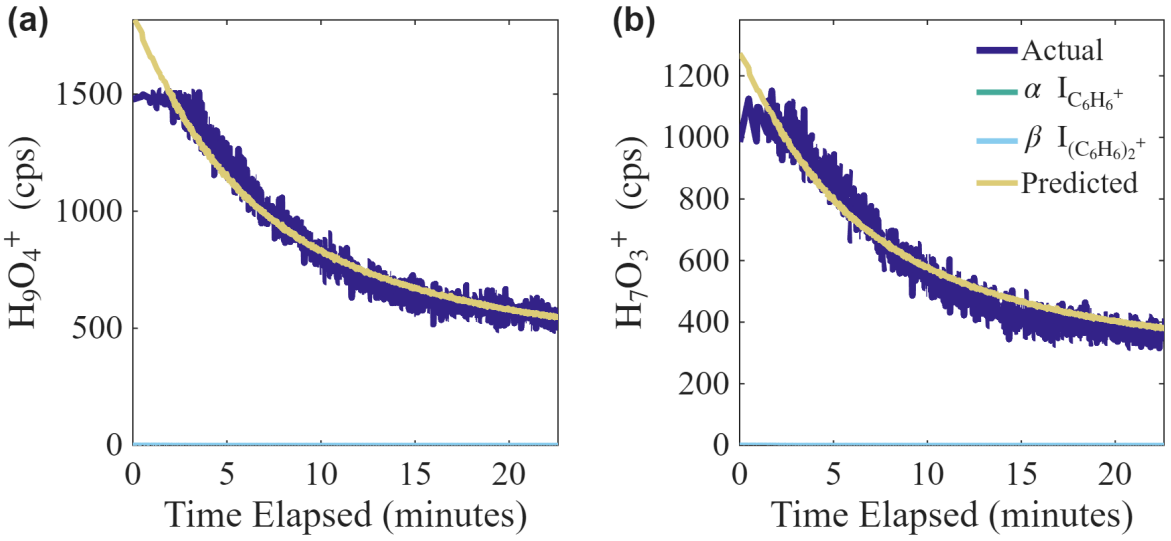

Figure S11. Estimation of α and β by varying the reagent ions $C_6H_6^+$ and $(C_6H_6)_2^+$ concentrations for (a) $H_9O_4^+$ and (b) $H_7O_3^+$. The α $I_{C_6H_6^+}$line is not shown for the water clusters, because of $\beta = 0$ where the green line completely overlaps with yellow.

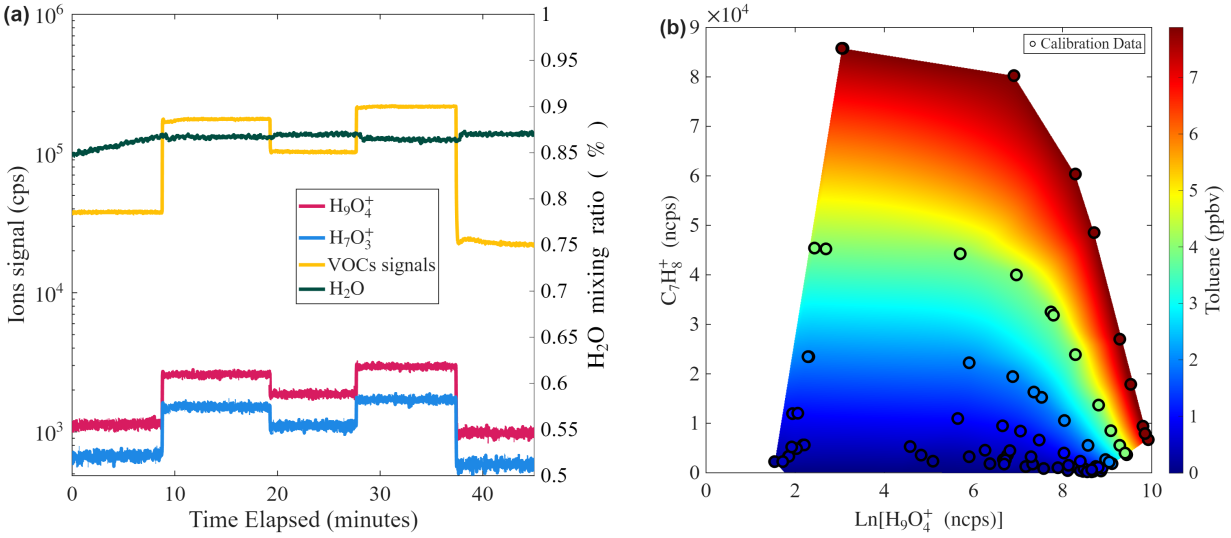

Figure S12. (a) Time series of water mixing ratio summed signals of VOCs (Isoprene, DMS, MACR, 2-Methylfuran, Toluene, m-Xylene, and o-Cresol) and water (e.g., $H_7O_3^+$ and $H_9O_4^+$) during a calibration experiment where water mixing ratio is held constant while the summed mixing ratio of VOCs is varied. (b) Two-dimensional calibration contour interpolated from calibration points obtained in the humidity-dependent calibration of toluene.

200 covalent bicyclic compound. Given that both isoprene and MACR contain conjugated double bonds similar to 1,3-butadiene, their reactions with $C_6H_6^+$ may likewise yield stable covalently bonded adducts (Figure S15).

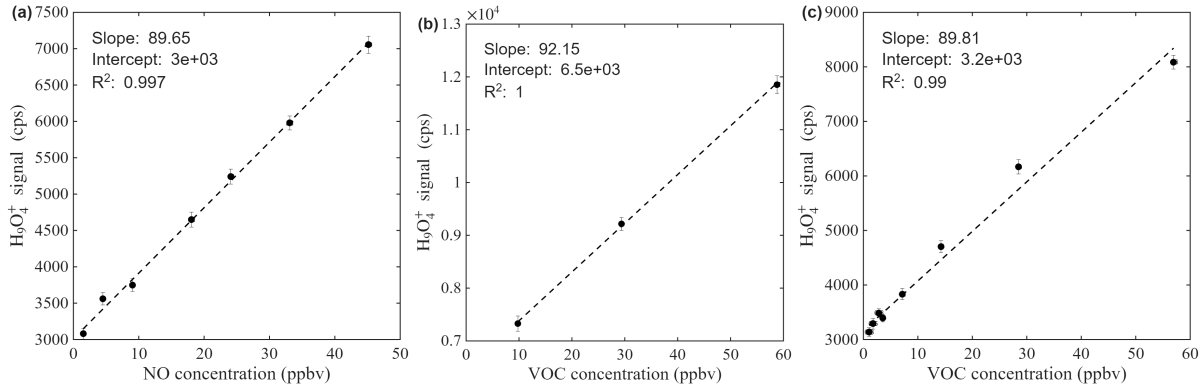

Figure S13. Change in $H_9O_4^+$ signals as a function of analyte concentrations. (a) NO at 1.6% H_2O mixing ratio. (b) VOCs (Isoprene, MCAR, Toluene, Chlorobenzene, o-Xylene, 1,3,5-TMB, Limonene, and D5 siloxane) at 2.7% H_2O mixing ratio. (c) VOCs (Isoprene, DMS, MACR, 2-Methylfuran, Toluene, m-Xylene, and o-Cresol) at 2% H_2O mixing ratio.

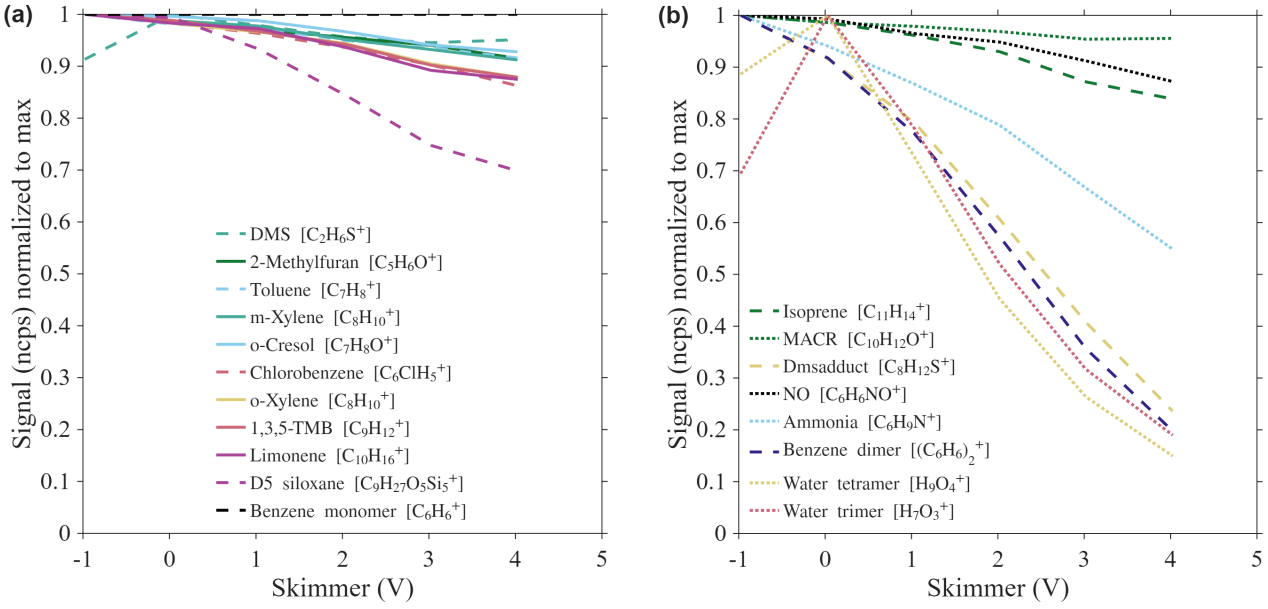

Figure S14. The dependence of analyte signal on the voltage gradient. The analyte signal is firstly normalized to $C_6H_6^+$ and then normalized to the maximum value. Normalized to $C_6H_6^+$ is to account for the systematic change in ion transmission efficiency due to changes in voltages of skimmer, BSQ front, and BSQ back. (a) Charge transfer ions. (b) Adduct ions. Solid, dashed, and dotted lines represent analytes in low IE class, mid IE class, and high IE class, respectively.

The relationship between the binding energies of adduct ions and ΔV_{50}, defined as the voltage gradient at which the product ion signal decreases to half of its maximum, is not straightforward. For example, the binding energy of DMS with $C_6H_6^+$ should be higher than that of NH_3 with $C_6H_6^+$ (113.1 vs. 78.7 kJ mol^{-1}). However, the observed ΔV_{50} for DMS is smaller than that

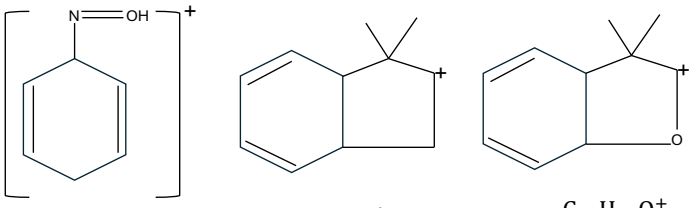

$C_6H_6NO^+$ $C_{11}H_{14}^+$ $C_{10}H_{12}O^+$

Figure S15. Possible structures for the benzene adducts of NO ($C_6H_6NO^+$), Isoprene ($C_{11}H_{14}^+$), and MACR ($C_{10}H_{12}O^+$)

for NH_3. This discrepancy may arise because increasing ΔV not only enhances CID but may also facilitate charge transfer for DMS, whose ionization energy is nearly identical to that of the benzene dimer.

We note that while both voltage scanning and instrument operating conditions (e.g., T, P, flow rate) influence ion signals, they do so through different mechanisms. Voltage scanning does not alter the ion chemistry within the IMR; its effects occur downstream, primarily impacting ion transmission and fragmentation in the ion optics. In contrast, instrument operating conditions directly affect the ion chemistry by altering reagent ion distribution and shifting reaction equilibria within the IMR.

3 Ambient measurements

3.1 Product ion classification into specific reaction pathways

Our benzene CIMS detected nearly 500 ions above the detection limit in field deployments. We use the ion chemical formula to infer their ionization pathways. Ions formed via proton transfer and hydride abstraction were grouped together, as they cannot be distinguished with this method. Importantly, the classification relies only on chemical formulas without explicitly considering charge (e.g., C_5H_8 is used to classify $C_5H_8^+$). The procedure is summarized in Figure S16. The first step separates ions by carbon number: fewer than six carbons versus more than six. For ions with fewer than six carbons, those with an even number of electrons are assigned to charge transfer, while those with an odd number are assigned to proton transfer/hydride abstraction. For ions with more than six carbons, we subtract C_6H_6 from the ion formula and analyze the residual formula. Ions are categorized as adducts if the residual formula contains multiple heteroatoms (e.g., NO, NH) or if its degree of unsaturation is greater than zero (e.g., C_5H_8, C_4H_6O). The remaining ions are classified as either charge transfer or proton transfer/hydride abstraction based on electron count of raw chemical formula. This classification is approximate, as it does not account for possible declustering.

3.2 PICARRO

We monitored the water mixing ratio of sample using a PICARRO model G2401 gas concentration analyzer, a commercial instrument designed to measure concentrations of CO_2, CH_4, CO, and H_2O. It operates based on Wavelength-Scanned Cavity

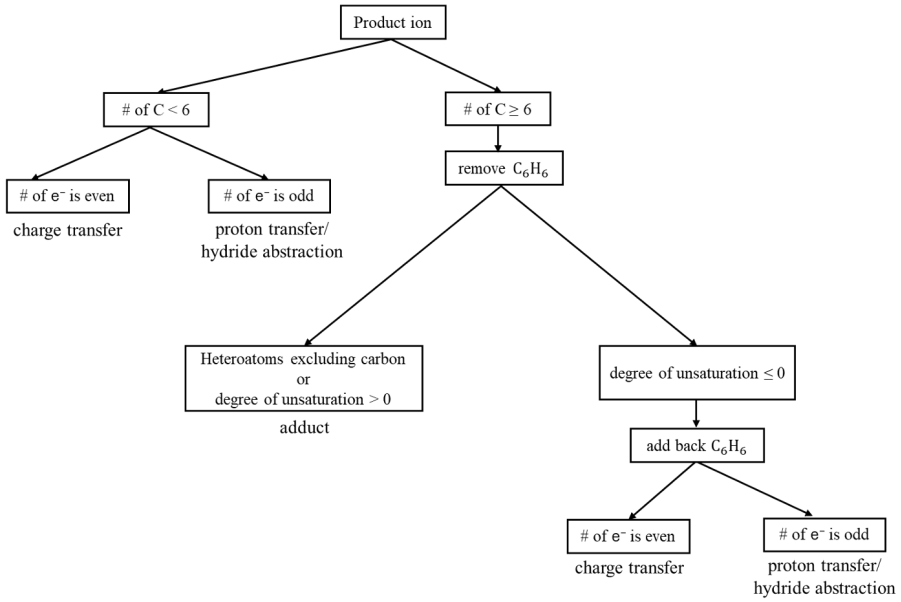

Figure S16. Flow diagram showing the classification of the analytes into possible charge transfer, proton transfer/hydride abstraction and adduct product ions.

Ring-Down Spectroscopy (WS-CRDS), a time-dependent technique that utilizes a near-infrared laser to determine the spectral signature of the target molecules. The analyzer circulates gas within an optical measurement cavity with a path length of up to 20 km. A proprietary high-precision wavelength monitor ensures only the relevant spectral features are observed, minimizing sensitivity to interfering gas species. This capability enables the instrument to perform ultra-trace gas concentration measurements in the presence of other gases, resulting in high linearity, precision, and accuracy under varying environmental conditions with minimal calibration requirements.

3.3 GC-PID

We deployed a gas chromatograph with photoionization detection (GC-PID, SRI model 8610C) alongside the benzene CIMS to provide in situ measurements of a suite of VOCs, including isoprene, toluene, α-pinene, and benzene. This GC-PID uses a Tenax sample trap, a 15 mm MXT-WAX precolumn for water removal, and two columns (30 mm MXT-Alumina column and 30 mm MXT-624 column) for separation. Each separation column is connected to a photoionization detector. UHP N_2 is used as carrier gas. Ambient air is sampled through the trap for 10 min. Then the trapped analyte elute was sent to the the MXT-Alumina column in the first 4.7 minutes and then to the MXT-624 column in the following 15.3 minutes. The chromatographic separation in columns is achieved using a specific oven temperature program, where the oven is initially held at $50°C$ for 5 minutes, then ramped at a rate of $20°C$ per minute to a final temperature of $180°C$. A 5-minute cooldown period between runs allows the oven to return to its initial temperature. Each GC cycle lasts for 25 minutes. Under these conditions, isoprene is

detected through the MXT-Alumina column at a retention time of approximately 13 minutes. The sensitivity of isoprene is 0.6508 area pptv^{-1} and was calibrated using the same VOC cylinder as benzene CIMS.

References

Aggarwal, S., Bansal, P., Wang, Y., Jorga, S., Macgregor, G., Rohner, U., Bannan, T., Salter, M., Zieger, P., Mohr, C., and Lopez-Hilfiker, F.: Identifying key parameters that affect sensitivity of flow tube chemical ionization mass spectrometers, EGUsphere, pp. 1–35, https://doi.org/10.5194/egusphere-2025-696, publisher: Copernicus GmbH, 2025.

Allgood, C., Lin, Y., Ma, Y.-C., and Munson, B.: Benzene as a selective chemical ionization reagent gas, Organic Mass Spectrometry, 25, 497–502, https://doi.org/10.1002/oms.1210251003, _eprint: https://onlinelibrary.wiley.com/doi/pdf/10.1002/oms.1210251003, 1990.

Bertram, T. H., Kimmel, J. R., Crisp, T. A., Ryder, O. S., Yatavelli, R. L. N., Thornton, J. A., Cubison, M. J., Gonin, M., and Worsnop, D. R.: A field-deployable, chemical ionization time-of-flight mass spectrometer, Atmospheric Measurement Techniques, 4, 1471–1479, https://doi.org/10.5194/amt-4-1471-2011, publisher: Copernicus GmbH, 2011.

Collin, J. E. and Franskin, M. J.: IONIZATION, DISSOCIATION, AND INTRAMOLECULAR REARRANGEMENTS IN ALIPHATIC AMINES UNDER ELECTRON BOMBARDMENT. CASE OF METHYLAMINE AND METHYLAMINE-Nd$sub2$, Bull. Soc. Roy. Sci. Liege, Vol: 35, https://www.osti.gov/biblio/4511668, 1966.

Harris, D., McKinnon, S., and Boyd, R. K.: The origins of the base peak in the electron impact spectrum of limonene, Organic Mass Spectrometry, 14, 265–272, https://doi.org/https://doi.org/10.1002/oms.1210140507, 1979.

Holman, R., Rozeboom, M., Gross, M., and Warner, C.: Mass spectrometry for investigations of gas-phase radical cation chemistry, Tetrahedron, 42, 6235–6244, https://doi.org/10.1016/S0040-4020(01)88085-6, 1986.

Ibrahim, Y. M., Meot-Ner, M., Alshraeh, E. H., El-Shall, M. S., and Scheiner, S.: Stepwise Hydration of Ionized Aromatics. Energies, Structures of the Hydrated Benzene Cation, and the Mechanism of Deprotonation Reactions, J. Am. Chem. Soc., 127, 7053–7064, https://doi.org/10.1021/ja050477g, 2005.

Ketkar, S. N., Dulak, J. G., Dheandhanoo, S., and Fite, W. L.: Benzene charge exchange at atmospheric pressure for low-level detection of pollutants in ambient air, Analytica Chimica Acta, 245, 267–270, https://doi.org/10.1016/S0003-2670(00)80231-7, 1991.

Kim, M. J., Zoerb, M. C., Campbell, N. R., Zimmermann, K. J., Blomquist, B. W., Huebert, B. J., and Bertram, T. H.: Revisiting benzene cluster cations for the chemical ionization of dimethyl sulfide and select volatile organic compounds, Atmospheric Measurement Techniques, 9, 1473–1484, https://doi.org/10.5194/amt-9-1473-2016, publisher: Copernicus GmbH, 2016.

Krechmer, J., Lopez-Hilfiker, F., Koss, A., Hutterli, M., Stoermer, C., Deming, B., Kimmel, J., Warneke, C., Holzinger, R., Jayne, J., Worsnop, D., Fuhrer, K., Gonin, M., and de Gouw, J.: Evaluation of a New Reagent-Ion Source and Focusing Ion–Molecule Reactor for Use in Proton-Transfer-Reaction Mass Spectrometry, Anal. Chem., 90, 12 011–12 018, https://doi.org/10.1021/acs.analchem.8b02641, publisher: American Chemical Society, 2018.

Lavi, A., Vermeuel, M. P., Novak, G. A., and Bertram, T. H.: The sensitivity of benzene cluster cation chemical ionization mass spectrometry to select biogenic terpenes, Atmospheric Measurement Techniques, 11, 3251–3262, https://doi.org/10.5194/amt-11-3251-2018, publisher: Copernicus GmbH, 2018.

Leibrock, E. and Huey, L. G.: Ion chemistry for the detection of isoprene and other volatile organic compounds in ambient air, Geophysical Research Letters, 27, 1719–1722, https://doi.org/10.1029/1999GL010804, _eprint: https://onlinelibrary.wiley.com/doi/pdf/10.1029/1999GL010804, 2000.

Leibrock, E., Huey, L. G., Goldan, P. D., Kuster, W. C., Williams, E., and Fehsenfeld, F. C.: Ground-based intercomparison of two isoprene measurement techniques, Atmospheric Chemistry and Physics, 3, 67–72, https://doi.org/10.5194/acp-3-67-2003, publisher: Copernicus GmbH, 2003.

Linstrom, P. J., Mallard, W. G., and National Institute of Standards and Technology (U.S.): NIST chemistry webbook, NIST standard reference database; 69, National Institute of Standards and Technology, Gaithersburg MD, 20899, http://webbook.nist.gov/chemistry/, 1997.

Lopez-Hilfiker, F. D., Iyer, S., Mohr, C., Lee, B. H., D'Ambro, E. L., Kurtén, T., and Thornton, J. A.: Constraining the sensitivity of iodide adduct chemical ionization mass spectrometry to multifunctional organic molecules using the collision limit and thermodynamic stability of iodide ion adducts, Atmospheric Measurement Techniques, 9, 1505–1512, https://doi.org/10.5194/amt-9-1505-2016, publisher: Copernicus GmbH, 2016.

Lossing, F. P., Lam, Y.-T., and Maccoll, A.: Gas phase heats of formation of alkyl immonium ions, Canadian Journal of Chemistry, 59, 2228–2231, https://doi.org/10.1139/v81-322, 1981.

MacDougall, D., Crummett, W. B., and Et Al., .: Guidelines for data acquisition and data quality evaluation in environmental chemistry, Anal. Chem., 52, 2242–2249, https://doi.org/10.1021/ac50064a004, 1980.

Meot-Ner, M., Hamlet, P., Hunter, E. P., and Field, F. H.: Bonding energies in association ions of aromatic compounds. Correlations with ionization energies, J. Am. Chem. Soc., 100, 5466–5471, https://doi.org/10.1021/ja00485a034, 1978.

Miller, D. L. and Gross, M. L.: Mechanism of the gas-phase reaction of the benzene radical cation and various alkyl iodides, J. Am. Chem. Soc., 105, 3783–3788, https://doi.org/10.1021/ja00350a005, 1983.

Mizuse, K., Hasegawa, H., Mikami, N., and Fujii, A.: Infrared and Electronic Spectroscopy of Benzene-Ammonia Cluster Radical Cations $[C_6\ H_6\ (NH_3\ )_{1,2}\ ]^+$: Observation of Isolated and Microsolvated σ-Complexes, J. Phys. Chem. A, 114, 11 060–11 069, https://doi.org/10.1021/jp1009466, 2010.

Mungall, E. L., Croft, B., Lizotte, M., Thomas, J. L., Murphy, J. G., Levasseur, M., Martin, R. V., Wentzell, J. J. B., Liggio, J., and Abbatt, J. P. D.: Dimethyl sulfide in the summertime Arctic atmosphere: measurements and source sensitivity simulations, Atmospheric Chemistry and Physics, 16, 6665–6680, https://doi.org/10.5194/acp-16-6665-2016, publisher: Copernicus GmbH, 2016.

Pagonis, D., Sekimoto, K., and de Gouw, J.: A Library of Proton-Transfer Reactions of H3O+ Ions Used for Trace Gas Detection, Journal of the American Society for Mass Spectrometry, 30, 1330–1335, https://doi.org/10.1007/s13361-019-02209-3, pMID: 31037568, 2019.

Reents, W. D. J. and Freiser, B. S.: Gas-phase nitrosation of benzene. Implications for solution electrophilic aromatic substitution reactions, J. Am. Chem. Soc., 102, 271–276, https://doi.org/10.1021/ja00521a043, publisher: American Chemical Society, 1980.

Riva, M., Pospisilova, V., Frege, C., Perrier, S., Bansal, P., Jorga, S., Sturm, P., Thornton, J. A., Rohner, U., and Lopez-Hilfiker, F.: Evaluation of a reduced-pressure chemical ion reactor utilizing adduct ionization for the detection of gaseous organic and inorganic species, Atmospheric Measurement Techniques, 17, 5887–5901, https://doi.org/10.5194/amt-17-5887-2024, publisher: Copernicus GmbH, 2024.

Rusyniak, M., Ibrahim, Y., Alsharaeh, E., Meot-Ner (Mautne, M., and El-Shall, M. S.: Mass-Selected Ion Mobility Studies of the Isomerization of the Benzene Radical Cation and Binding Energy of the Benzene Dimer Cation. Separation of Isomeric Ions by Dimer Formation, J. Phys. Chem. A, 107, 7656–7666, https://doi.org/10.1021/jp034850n, publisher: American Chemical Society, 2003.

Schobesberger, S., D'Ambro, E. L., Vettikkat, L., Lee, B. H., Peng, Q., Bell, D. M., Shilling, J. E., Shrivastava, M., Pekour, M., Fast, J., and Thornton, J. A.: Airborne flux measurements of ammonia over the southern Great Plains using chemical ionization mass spectrometry, Atmospheric Measurement Techniques, 16, 247–271, https://doi.org/10.5194/amt-16-247-2023, publisher: Copernicus GmbH, 2023.

Sieck, L. W. and Gorden, R.: Formation of dimeric parent cations in aromatic hydrocarbons, International Journal of Mass Spectrometry and Ion Physics, 19, 269–286, https://doi.org/10.1016/0020-7381(76)80011-3, 1976.

Solka, B. H. and Russell, M. E.: Energetics of formation of some structural isomers of gaseous C2H5O+ and C2H6N+ ions, The Journal of Physical Chemistry, 78, 1268–1273, https://doi.org/10.1021/j100606a007, 1974.

Stone, J. A. and Lin, M. S.: The formation and reactions of aromatic dimer cations in a high pressure photoionization source, Can. J. Chem., 58, 1666–1672, https://doi.org/10.1139/v80-266, publisher: NRC Research Press, 1980.

Su, T.: Parametrization of kinetic energy dependences of ion–polar molecule collision rate constants by trajectory calculations, The Journal of Chemical Physics, 100, 4703, https://doi.org/10.1063/1.466255, 1994.

Subba Rao, S. C. and Fenselau, C.: Evaluation of benzene as a charge exchange reagent, Anal. Chem., 50, 511–515, https://doi.org/10.1021/ac50025a036, publisher: American Chemical Society, 1978.

Tomoda, S. and Kimura, K.: Ionization energies and hydrogen-bond strength of the water clusters, Chemical Physics Letters, 102, 560–564, https://doi.org/10.1016/0009-2614(83)87466-1, 1983.

Vermeuel, M. P.: The Influence of Complex Meteorology and Surface Heterogeneity on Oxidation in the Troposphere, Ph.D., The University of Wisconsin - Madison, United States – Wisconsin, https://www.proquest.com/dissertations-theses/influence-complex-meteorology-surface/docview/2511403096/se-2?accountid=15159, iSBN: 9798597065342 Publication Title: ProQuest Dissertations and Theses 28318994, 2021.

Xu, L., Coggon, M. M., Stockwell, C. E., Gilman, J. B., Robinson, M. A., Breitenlechner, M., Lamplugh, A., Crounse, J. D., Wennberg, P. O., Neuman, J. A., Novak, G. A., Veres, P. R., Brown, S. S., and Warneke, C.: Chemical ionization mass spectrometry utilizing ammonium ions (NH_4^+ CIMS) for measurements of organic compounds in the atmosphere, Atmospheric Measurement Techniques, 15, 7353–7373, https://doi.org/10.5194/amt-15-7353-2022, publisher: Copernicus GmbH, 2022.